

Open-Set LiDAR Panoptic Segmentation Guided by Uncertainty-Aware Learning

Rohit Mohan¹, Julia Hindel¹, Florian Drews², Claudius Gläser², Daniele Cattaneo¹, Abhinav Valada¹

Abstract—Autonomous vehicles that navigate in open-world environments may encounter previously unseen object classes. However, most existing LiDAR panoptic segmentation models rely on closed-set assumptions, failing to detect unknown object instances. In this work, we propose ULOPS, an uncertainty-guided open-set panoptic segmentation framework that leverages Dirichlet-based evidential learning to model predictive uncertainty. Our architecture incorporates separate decoders for semantic segmentation with uncertainty estimation, embedding with prototype association, and instance center prediction. During inference, we leverage uncertainty estimates to identify and segment unknown instances. To strengthen the model’s ability to differentiate between known and unknown objects, we introduce three uncertainty-driven loss functions. Uniform Evidence Loss to encourage high uncertainty in unknown regions. Adaptive Uncertainty Separation Loss ensures a consistent difference in uncertainty estimates between known and unknown objects at a global scale. Contrastive Uncertainty Loss refines this separation at the fine-grained level. To evaluate open-set performance, we extend benchmark settings on KITTI-360 and introduce a new open-set evaluation for nuScenes. Extensive experiments demonstrate that ULOPS consistently outperforms existing open-set LiDAR panoptic segmentation methods. We make the code available at <http://ulops.cs.uni-freiburg.de>.

I. INTRODUCTION

Accurate scene understanding [1], [2] plays a central role in autonomous driving, forming the foundation for safe navigation [3] and enhancing downstream tasks such as localization [4], [5]. LiDAR 3D panoptic segmentation plays a crucial role in this task by detecting both semantic classes and individual object instances. However, models for LiDAR panoptic segmentation are typically trained on a closed-set of predefined categories [6]. This constraint limits adaptability in open-world environments where novel objects frequently appear [7], [8].

Standard closed-set models tend to confidently misclassify unknown classes as known ones, leading to inaccurate perception and potential safety risks [9]–[13]. Addressing this challenge requires a shift toward open-set panoptic segmentation, as shown in Fig. 1. While this task has been extensively studied in computer vision [14]–[16], its potential for 3D scene understanding remains largely unexplored. One of the first efforts in this direction was OSIS [17]. It introduced open-set instance segmentation for 3D point clouds by clustering points in a category-agnostic embedding space. This allowed segmentation of both known and unknown objects. However, OSIS relies only on feature-space clustering and

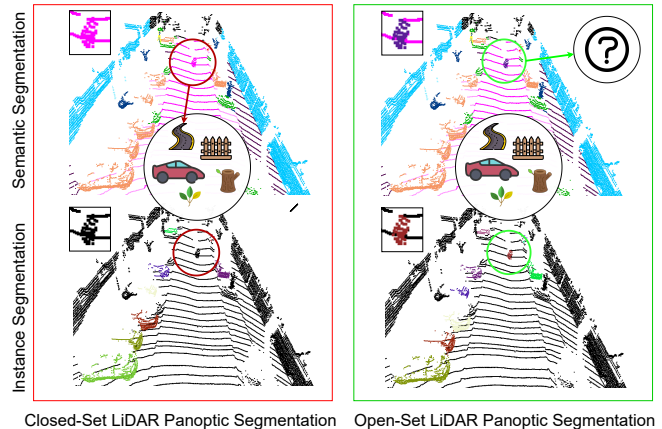


Fig. 1. Illustration of the comparison between closed-set and open-set LiDAR panoptic segmentation. In closed-set panoptic segmentation (left), models are limited to predefined categories and misclassify novel objects as known classes, leading to incorrect predictions. In open-set panoptic segmentation (right), models distinguish unknown objects from known categories, enabling reliable scene understanding in open-world environments.

does not explicitly distinguish between known and unknown objects. Consequently, it struggles to separate novel instances from background noise or unstructured regions in the scene. Following this, OWL [18] extended open-set recognition to panoptic segmentation. It proposed a framework that first classifies points into known stuff, known things, and unknown categories. After classification, it groups unknown and thing instances. However, inspired by [19], OWL relies on a fixed “other” category to represent unknowns during training. This limits its ability to generalize and adapt to truly novel objects.

To address the limitations of existing approaches, we propose ULOPS, an uncertainty-guided open-set panoptic segmentation framework for LiDAR point clouds. ULOPS explicitly models uncertainty using Dirichlet-based evidential learning, enabling the network to dynamically identify unknown objects at inference time. We introduce a multi-task architecture with three decoders: a semantic segmentation decoder that predicts class labels while quantifying uncertainty, an embedding decoder that learns instance-aware representations, and an instance center decoder that detects object centers. Crucially, we formulate three uncertainty-driven loss functions to reinforce the network’s ability to distinguish between known and unknown regions. Uniform Evidence Loss guides the model to assign high uncertainty to unknown regions, Adaptive Uncertainty Separation Loss ensures a consistent difference in uncertainty estimates between known and unknown objects at a global level, while Contrastive Uncertainty Loss reinforces this separation at

¹ Department of Computer Science, University of Freiburg, Germany

² Bosch Research, Robert Bosch GmbH, Renningen, Germany

This work was funded by Bosch Research for AI-driven automated driving.

the individual sample level. Further, we complement prior work by introducing two novel panoptic open-set evaluation settings based on the KITTI-360 [20] and nuScenes [21] datasets.

Our main contributions can be summarized as follows:

- We propose ULOPS, an uncertainty-guided open-set panoptic segmentation framework for LiDAR point clouds.
- We design three novel uncertainty-driven loss functions that induce open-set model capabilities.
- Our approach outperforms established open-set LiDAR panoptic segmentation baselines, demonstrating superior capability in distinguishing known and unknown objects.
- We establish new benchmark settings for open-set LiDAR panoptic segmentation on KITTI-360 and Panoptic nuScenes.

II. RELATED WORK

LiDAR Panoptic Segmentation: LiDAR Panoptic Segmentation methods are typically categorized into single-stage and two-stage approaches. Both approaches rely on a backbone network to extract features from LiDAR point clouds, utilizing different representations such as points [22], voxels [23], range views [6], and bird’s-eye views [24], [25]. Two-stage methods [6], [26] fuse instance segmentation outputs from a proposal-based branch with a separate semantic segmentation branch to yield unified panoptic predictions. Single-stage approaches, on the other hand, generate instance predictions using either deterministic methods [27], [28] or clustering mechanisms that rely on learnable representations [29]. Recent works [22], [30], inspired by the 2D panoptic segmentation model MaskFormer [31] predict instance masks and semantic labels in a single pass by employing learnable queries. PUPS [30] employs bipartite matching for point-level classification while MaskRange [32] transforms point clouds into a range-view representation to leverage MaskFormer-like architectures. while P3Former [22] integrate multi-scale voxel features and novel position embeddings. However, the outlined works are restricted to closed-world scenarios where all categories are observed during training. In this work, we introduce the integration of prototype-embedding association and uncertainty estimation in a single-stage approach to handle open-set scenarios in the LiDAR domain, enhancing segmentation robustness in complex and dynamic environments.

Open-Set Learning: Open-set perception has been extensively studied in classification tasks to tackle the challenge of encountering novel classes during inference [14]–[16]. To mitigate the limitations of softmax-based classifiers, OpenMax [33] re-calibrates classification scores to bound the risk associated with unknown classes. An alternative synthetic [34], [35] approach, G-OpenMax [36], employs generative models to synthesize data for unknown classes during training, enhancing the model’s capability to identify novel examples during inference. Further, deep generative adversarial networks [37], [38] and variational autoencoders (VAEs) [39], [40] have been leveraged to simulate unknown objects during training, reinforcing the model’s ability to

distinguish novel classes [41], [42]. Recent studies [43], [44] have demonstrated that predictive uncertainty is an effective scoring mechanism to identify objects that do not belong to any known class. For instance, DPN [45] utilizes Dirichlet distributions to capture uncertainty through probabilistic assignments, while Bayesian SSD [46] uses Monte Carlo Dropout to identify unknown objects during detection. Beyond object recognition, open-world recognition methods [47] dynamically label unknowns and incorporate them into subsequent training. In this work, we leverage predictive uncertainty to identify novel classes while proactively shaping the model’s understanding of unknown regions through local and global uncertainty-guided supervision during training, enabling a more structured and adaptive open-set perception.

Open-Set Panoptic Segmentation: Compared to its well-established closed-set counterpart, open-set panoptic segmentation remains a challenging task in both images and point clouds. In images, the pioneering model EOPSN [48] groups unlabeled objects across inputs. For LiDAR panoptic segmentation, OSIS [17] establishes open-set instance segmentation by learning a category-agnostic embedding space. A detection head localizes known objects, while a separately trained embedding head clusters unknown instances using association scores and DBSCAN. Further, OWL [18] proposes an open-set learning approach that employs $(K + 1)$ classification to capture rare and novel categories, followed by a hierarchical segmentation tree for clustering unknowns. The model is trained on the SemanticKITTI dataset, where some categories are labeled as unknown. Inference is then performed on KITTI-360. However, due to the semantic overlap between the two datasets, OWL is exposed to the same subset of unknown categories during training and inference. We believe that true open-set generalization requires a strict separation between the unknown categories encountered during training and those encountered during inference. Consequently, we propose a new vocabulary split, ensuring that SemanticKITTI classes are excluded from the unknown categories in KITTI-360.

III. ULOPS NETWORK ARCHITECTURE

In this section, we introduce our ULOPS architecture, illustrated in Fig. 3. We begin with an overview of the network before detailing its key components. Our framework is based on a backbone consisting of a stem that encodes the raw point cloud into a fixed-size 2D polar BEV representation, followed by a shared encoder that extracts high-level features. Next, we employ three decoders, each dedicated to a specific task: 1) a semantic segmentation decoder that generates semantic predictions along with uncertainty estimates, 2) an embedding decoder that learns instance-aware embeddings and prototypes, and 3) an instance center decoder that estimates class-agnostic object centers.

During inference, we combine these outputs to yield the final open-set panoptic segmentation. We first use the uncertainty estimates to separate known and unknown regions, labeling high-uncertainty areas as potential unknown objects. In lower-uncertainty (i.e., known) regions, instance-aware embeddings are associated with instance center prototypes to segment *thing* objects. Meanwhile, majority voting in

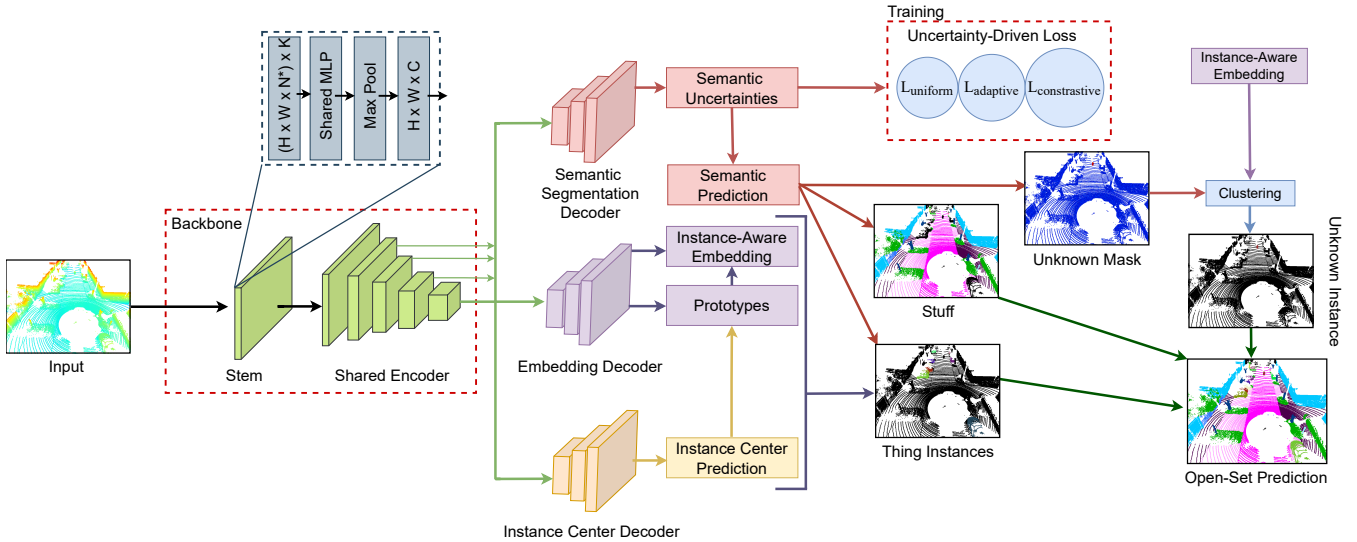


Fig. 2. Overview of the ULOPS architecture for open-set LiDAR panoptic segmentation. The input LiDAR point cloud is processed by a shared backbone, which extracts multi-scale features. Three task-specific decoders refine these features: the semantic segmentation decoder predicts class labels and uncertainty estimates, the embedding decoder generates instance-aware embeddings with prototype association, and the instance center decoder detects object centers. During inference, uncertainty estimates guide the separation of known and unknown regions. Then, known instances are segmented using instance embeddings and object centers, while unknown instances are clustered separately. Our framework is trained with uncertainty-driven loss functions to enforce structured separation between known and unknown objects, leading to robust open-set panoptic segmentation.

semantic prediction assigns semantic classes to these class-agnostic instances. For high-uncertainty regions, embeddings are clustered to identify unknown objects. During training, we encourage higher uncertainty for unknown regions through a set of specialized losses: Uniform Evidence Loss, Adaptive Uncertainty Separation Loss, and Contrastive Uncertainty Loss. By jointly optimizing these losses alongside the core panoptic segmentation objectives, the network is better equipped to distinguish between known and unknown objects in LiDAR scenes.

A. Backbone

Following PolarNet [24], we first convert the raw point cloud $\mathbf{P} \in \mathbb{R}^{N \times K}$ into a polar bird’s-eye view (BEV) grid of size $H \times W$, where H and W correspond to the radial and angular dimensions, respectively. Each grid cell accumulates points based on their 3D polar coordinates. We then employ a simplified PointNet-style module [49], which applies a series of linear transformations interleaved with batch normalization and ReLU activation. After processing each grid cell, we aggregate features along the vertical Z -dimension using max pooling, producing a fixed-size representation $\mathbf{M} \in \mathbb{R}^{H \times W \times C}$, where $C = 512$ is the feature dimension. We adopt polar rather than Cartesian coordinates to ensure a more balanced distribution of points over different ranges, helping the network focus on closer, denser areas without excessive quantization loss [24]. To capture multi-scale context, we employ a U-Net-style encoder [50] that progressively downsamples the BEV representation by a factor of $2\times$, $4\times$, $8\times$, and $16\times$. These feature maps are fed to the decoders, allowing the network to integrate both coarse global context and fine local details in subsequent segmentation and instance-level tasks.

B. Decoders

We employ three task-specific decoders for semantic segmentation, embedding, and instance center prediction. Each decoder follows a U-Net architecture [50] consisting of four upsampling stages. At each stage, feature maps are progressively upsampled and fused with the corresponding encoder outputs at the same resolution. This structure preserves coarse context from deeper layers while reintroducing fine-grained details from earlier encoder stages. While the overall decoding architecture remains consistent, the final layers and feature transformations are tailored to each task. In the following subsections, we provide a detailed explanation of these adaptations.

1) *Semantic Segmentation Decoder*: The semantic decoder yields class logits for the K known classes, along with an associated uncertainty, on a three-dimensional grid of size $Z \times H \times W$. Here, Z represents the number of bins in the voxelized 3D space, determining the resolution along the height axis. Specifically, for each (h, w) position in the BEV plane, it outputs a prediction of shape (Z, K) , where each vertical level z contains class logits for all K known categories. These logits are then reshaped into a 3D voxel representation. During training, each voxel’s ground-truth label is determined by majority voting among the raw LiDAR points that fall within that voxel. Rather than directly applying a softmax function and optimizing with cross-entropy loss, we adopt a Dirichlet-based learning framework [45] to explicitly model uncertainty. The standard cross-entropy loss would force the network to produce deterministic probability distributions, making it overconfident in ambiguous or unknown regions.

To address this limitation, the semantic decoder predicts Dirichlet parameters instead of class probabilities. Consequently, this decoder outputs strictly positive parameters

α_k via softplus activation, which represents a Dirichlet distribution $\text{Dir}(\alpha)$ over the class probabilities. We leverage evidence-based learning [45], where each class’s strength of association is captured by the evidence $e_k = \alpha_k - 1$. The total uncertainty is then derived as:

$$u = \frac{\sum_{k=1}^K \alpha_k}{K}, \quad (1)$$

which increases when a voxel lacks strong evidence for any known class. The network is optimized using the negative expected log-likelihood of the ground-truth class under the Dirichlet distribution:

$$\mathcal{L}_{\text{seg}} = \psi \left(\sum_{k=1}^K \alpha_k \right) - \psi(\alpha_y), \quad (2)$$

where ψ is the digamma function, and α_y corresponds to the voxel’s ground-truth class label y . By learning through the Dirichlet distribution, the model naturally distinguishes known from unknown objects, as voxels with low evidence across all known classes exhibit high uncertainty predictions.

2) *Embedding Decoder*: Similar to the semantic decoder, our embedding decoder outputs a 3D feature volume of shape $\phi_{\text{embed}} \in \mathbb{R}^{F \times Z \times H \times W}$. Here, F is the dimension of the embedding space. As in the semantic branch, voxel-aggregated training labels are assigned via majority voting of same-voxel raw LiDAR points. To facilitate instance-level grouping, we learn prototypes around object centers, which are taken from ground-truth annotations during training. Each prototype c is characterized by a mean $\mu_c \in \mathbb{R}^F$ and variance $\sigma_c^2 \in \mathbb{R}^+$. The voxel embeddings are then compared to these prototypes using a variance-scaled distance metric, producing an association score $S(v, c)$ [17] for each voxel–prototype pair:

$$S(v, c) = \exp \left(-\frac{\|\phi_v^{\text{embed}} - \mu_c\|^2}{2\sigma_c^2} \right), \quad (3)$$

where ϕ_v^{embed} is the embedding of a given voxel v . During inference, voxels are assigned to the prototype with the highest association score, grouping them into coherent thing instances. We employ a discriminative loss [51] to ensure that embeddings within the same instance form compact clusters while keeping different instances well separated. Additionally, we use a prototype loss [17] to align the learned prototypes with their corresponding object embeddings. We present the details of these losses in the supplementary material.

3) *Instance Center Decoder*: The instance center decoder produces a heatmap representing the likelihood of instance centers across the 3D grid of size $Z \times H \times W$. We assign each voxel a scalar value indicating its probability of being an instance center. Given that object centers may not align precisely with dense LiDAR points in the voxelized representation, we generate the ground-truth center map using a 3D Gaussian kernel centered at each instance’s mass centroid [28]. Specifically, the ground-truth heatmap is defined as:

$$H_v = \max_i \exp \left(-\frac{\|v - c_i\|^2}{2\sigma^2} \right), \quad (4)$$

where c_i denotes the centroid of instance i in the voxel space. During training, the predicted center heatmap \hat{H} is supervised using a mean squared error (MSE) loss:

$$\mathcal{L}_{\text{center}} = \frac{1}{N} \sum_v (\hat{H}_v - H_v)^2, \quad (5)$$

where N is the total number of voxels in the grid. The local maxima in the predicted heatmap \hat{H} are identified as instance centers which are subsequently used to guide instance grouping in the embedding decoder.

C. Inference

To achieve open-set panoptic segmentation, we sequentially fuse outputs from the semantic segmentation, embedding, and instance center decoders in three steps. First, unknown regions are identified by thresholding the predicted uncertainty map, where a voxel is classified as unknown if its uncertainty $u(v)$ exceeds an adaptive threshold, i.e., $u(v) \geq \mu_u + t \cdot \sigma_u$, where μ_u and σ_u are the mean and standard deviation of uncertainties, and t controls sensitivity to unknown objects.

Next, we perform instance segmentation for known objects by assigning voxels to the nearest predicted center by leveraging the association scores computed in the embedding decoder. We determine the semantic labels through majority voting of the semantic predictions of within each voxel. Finally, following [17], we apply DBSCAN [52] clustering to the embeddings of the embedding decoder to segment distinct instances for unknown voxels.

D. Uncertainty-Driven Losses for Unknown Segmentation

To ensure the network computes high uncertainty scores for unknown (open-set) regions, we propose three complementary uncertainty losses: Uniform Evidence Loss, Adaptive Uncertainty Separation Loss, and Contrastive Uncertainty Loss. These losses are applied to the semantic decoder’s output and are computed based on ground-truth unknown labels. Drawing inspiration from evidential deep learning [43] and open-set recognition [53], these losses minimize known class confidence in unknown regions, thereby improving unknown class segmentation at inference time.

a) *Uniform Evidence Loss*: For each voxel labeled as unknown in the training data (i.e., not belonging to any of the K known classes), we encourage the Dirichlet parameters to be close to $\alpha_k \approx 1$. Equivalently, this implies zero evidence ($\alpha_k - 1 \approx 0$) for all known classes. Concretely, we use a mean-squared error (MSE) penalty:

$$\mathcal{L}_{\text{uniform}} = \|\alpha_{\text{unknown}} - \mathbf{1}\|^2, \quad (6)$$

where α_{unknown} represents the vector of Dirichlet parameters for an unknown voxel, and $\mathbf{1}$ is a vector of ones. This voxel-wise loss ensures that each unknown voxel’s evidence $\alpha_k - 1$ remains close to zero. This simple formulation increases the local uncertainty whenever the voxel represents the unknown class, resulting in a flat (maximally uncertain) Dirichlet distribution. However, since this loss is independently applied for each voxel, it does not account for the global distribution of uncertainty in the scene.

b) *Adaptive Uncertainty Separation Loss*: While uniform evidence loss enforces high per-voxel uncertainty for unknowns, it does not explicitly ensure a clear separation between the uncertainties of known and unknown voxels. To complement the uniform evidence loss, our adaptive variant uses global statistics to modulate the push for higher uncertainty. We track the mean uncertainty over known (μ_{known}) and unknown (μ_{unknown}) voxels within each batch:

$$\Delta u = (\mu_{\text{unknown}}(u)) - (\mu_{\text{known}}(u)), \quad (7)$$

and employ a decaying function of Δu defined as:

$$\mathcal{L}_{\text{adaptive}} = \exp\left(-\frac{\Delta u}{\sigma_{\text{known}}}\right), \quad (8)$$

where σ_{known} is the standard deviation of the uncertainty for known voxels. This loss is combined with a training schedule (e.g., an epoch-based weight) to avoid over-penalizing the model once it learns to distinguish known and unknown voxels effectively. This ensures that unknown voxels not only exhibit high uncertainty but are also consistently more uncertain than known voxels. Our loss differs from typical margin-based approaches by considering the distribution of uncertainties on the known classes at each training step. By combining both losses, we enforce high uncertainty at the voxel level (Uniform Evidence Loss) while ensuring a meaningful separation between known and unknown uncertainties at a global level.

c) *Contrastive Uncertainty Loss*: While adaptive uncertainty separation loss ensures a global distinction between known and unknown uncertainties, it does not explicitly enforce per-instance separation. Additionally, Uniform Evidence Loss ensures high uncertainty for unknown regions, but it does so without enforcing a clear relative separation between known and unknown uncertainties. This means that while unknown voxels have high uncertainty, their values may still overlap with certain known voxels, particularly in regions with high intra-class variation. Motivated by contrastive open-set learning [53], we explicitly compare the uncertainty of known vs. unknown voxels. We sample pairs of (known, unknown) voxels within a batch and enforce $u_{\text{unknown}} > u_{\text{known}} + \delta$, where δ is a margin. In practice, we subtract δ from the pairwise difference and apply a negative log-sigmoid:

$$\mathcal{L}_{\text{contrastive}} = -\log(\sigma(u_{\text{unknown}} - u_{\text{known}} - \delta)), \quad (9)$$

such that the loss decreases as unknown uncertainty exceeds known uncertainty by at least δ . This strategy differs from [53] primarily in what is being contrasted: rather than embedding distances, we contrast uncertainty values in our Dirichlet-based segmentation framework. This ensures that any voxel labeled as unknown achieves a distinctly higher uncertainty than any voxel from the known classes.

IV. EXPERIMENTAL EVALUATION

In this section, we first outline the datasets used for evaluation, followed by the training protocol and benchmarking results. We then conduct ablation studies on different types of uncertainty estimation and the proposed losses, and provide a qualitative analysis.

A. Datasets

Following [18], we train on SemanticKITTI [54] and evaluate its open-set performance on KITTI-360 [20]. Both datasets were collected using the same sensor setup in the same city but in different, non-overlapping districts. As KITTI-360 introduces greater variation in unknown classes, its evaluation setup serves as a proxy for LiDAR open-set panoptic segmentation performance. We assess performance on the two vocabulary settings proposed in [18]. Vocabulary 1 consists of 6 stuff classes, 3 thing classes, and 1 unknown class, while Vocabulary 2 includes 10 stuff classes, 5 thing classes, and 1 unknown class.

Additionally, we also report results on SemanticKITTI for completeness. However, due to semantic overlap between the unknown categories of SemanticKITTI and KITTI-360, the standard evaluation setting does not fully measure the impact of truly unseen unknown objects during training. To address this, we introduce a vocabulary referred to as Vocabulary Unseen by modifying Vocabulary 1 for evaluation on KITTI-360, where we exclude unknown semantic classes shared between the two datasets, namely, bicycle, motorcycle, other-vehicle, trunk, pole, traffic-sign, other-structure, other-object, other-ground, and parking. This setup ensures a stricter separation of training and inference unknowns, providing a more comprehensive assessment of open-set generalization.

In addition to SemanticKITTI and KITTI-360, we further evaluate our approach on nuScenes [21], a large-scale dataset for LiDAR panoptic segmentation in urban driving scenarios. This evaluation assesses the model’s open-set generalization across a dataset with diverse scene compositions and object distributions. Our defined panoptic open-set vocabulary includes the following thing classes: car, truck, and pedestrian, and stuff classes: road, sidewalk, terrain, manmade, and vegetation. We include bus, construction vehicle, bicycle, motorcycle, and other flat surfaces as unknown categories in the evaluation. Meanwhile, we designate barrier, traffic cone, and trailer as unknown categories during training. In total, our setup consists of three thing classes, five stuff classes, and one unknown class.

B. Training Protocol

We discretize the 3D space to $[480, 360, 32]$ voxels for SemanticKITTI ($r : 1 \sim 60 \text{ m}, z : -3 \sim 3 \text{ m}$) and for nuScenes ($r : 0 \sim 50 \text{ m}, z : -5 \sim 3 \text{ m}$), where r denotes the radial distance from the LiDAR sensor. The network is trained for 60 epochs with a batch size of 4 and a crop size of $[240, 180, 32]$. We use the Adam optimizer with an initial learning rate of 0.01, with stepwise decay by a factor of 10 at 45 and 55 epochs. We apply instance augmentation along with random point cloud augmentations (flipping, rotation, scaling). We set $t = 3$ for the uncertainty threshold and $F = 32$ for the embedding size. Loss weights are set as follows: $\mathcal{L}_{\text{center}} = 200$, $\mathcal{L}_{\text{uniform}} = 0.1$, $\mathcal{L}_{\text{adaptive}} = 0.1$, and $\mathcal{L}_{\text{contrastive}} = 0.7$, with all other losses weighted at 1.

C. Benchmarking Results

In Tab. I, we compare the performance of our ULOPS with 4D-PLS [28], PolarSeg-Panoptic [27], and OWL [18] on the

TABLE I

OPEN-SET LiDAR PANOPTIC SEGMENTATION RESULTS ON SEMANTICKITTI AND KITTI-360 USING VOCABULARIES FROM [18].

	Method	Known			Unknown			
		PQ	PQ Th	PQ St	UQ	Recall	SQ	
Vocabulary 1	SemKITTI	4D-PLS [28]	67.8	60.0	71.7	7.8	10.8	71.9
		PolarSeg-Panoptic [27]	68.6	68.2	68.8	10.2	14.7	69.3
		OWL [18]	69.4	64.7	71.7	39.6	48.4	81.8
		ULOPS (Ours)	70.5	68.9	71.3	41.9	50.6	82.3
	KITTI-360	4D-PLS [28]	56.1	56.2	56.0	1.3	2.0	65.7
		PolarSeg-Panoptic [27]	0.7	0.7	0.7	0.0	0.1	76.4
		OWL [18]	59.4	66.2	56.0	36.3	45.1	80.5
		ULOPS (Ours)	60.6	67.1	57.4	38.6	47.3	80.9
Vocabulary 2	SemKITTI	4D-PLS [28]	60.2	57.9	61.4	16.4	22.2	73.8
		PolarSeg-Panoptic [27]	58.6	56.5	55.2	14.9	20.7	72.1
		OWL	61.9	62.9	61.4	49.3	57.0	86.3
		ULOPS (Ours)	62.1	64.1	61.1	50.1	59.6	87.1
	KITTI-360	4D-PLS [28]	45.9	47.9	44.8	3.4	4.9	69.8
		PolarSeg-Panoptic [27]	1.2	0.4	1.6	0.0	0.0	71.1
		OWL	53.4	55.1	52.5	21.2	26.8	79.0
		ULOPS (Ours)	55.0	58.3	53.4	25.9	28.5	79.7

Superscripts Th and St refer to *thing* and *stuff* classes, respectively. All metrics are reported in %.

TABLE II

COMPARISON OF PANOPTIC nuScENES USING VOCABULARY AS DESCRIBED IN SEC. IV-A.

Method	Known			Unknown		
	PQ	PQ Th	PQ St	UQ	Recall	SQ
4D-PLS [28]	70.7	64.3	73.9	8.3	4.8	68.3
PolarSeg-Panoptic [27]	71.5	70.1	72.3	5.7	3.7	67.2
OWL [18]	71.6	67.2	73.9	18.9	20.7	69.3
ULOPS (Ours)	72.1	70.6	72.8	27.3	30.6	71.2

Superscripts Th and St refer to *thing* and *stuff* classes, respectively. All metrics are reported in %.

SemanticKITTI and KITTI-360 datasets using two different vocabularies. Our evaluation considers multiple metrics, including Panoptic Quality (PQ) [18] for known classes (split into PQTh for things and PQSt for stuff), as well as Unknown Quality (UQ) [18], recall, and Segmentation Quality (SQ) for unknown regions. Overall, our approach consistently outperforms all baselines, particularly in identifying and segmenting unknown objects. On SemanticKITTI (Vocabulary 1), methods relying solely on K+1 supervision (such as 4D-PLS [28] and PolarSeg-Panoptic [27]) struggle to generalize beyond the known categories. This is evident given the diverse nature of unknown objects in the dataset, ranging from bicycles to traffic signs and tree trunks, resulting in low unknown detection scores.

The problem is even more pronounced in KITTI-360, where the range of unknown objects is significantly larger, further widening the performance gap. In contrast, OWL and our approach, both designed for open-set segmentation, perform significantly better for both known and unknown classes. While OWL and our method both apply clustering to obtain instances, our method achieves a superior performance due to explicitly modeled uncertainty estimation, which divides known and unknown categories. Our uncertainty-driven losses encourage the network to better recognize

TABLE III

PERFORMANCE COMPARISON ON KITTI-360 WITH OUR PROPOSED VOCABULARY UNSEEN AS DESCRIBED IN SEC. IV-A.

Method	Known			Unknown		
	PQ	PQ Th	PQ St	UQ	Recall	SQ
4D-PLS [28]	57.2	57.1	57.3	1.1	2.2	66.9
PolarSeg-Panoptic [27]	0.9	0.9	0.9	0	0.1	76.2
OWL [18]	60.7	67.5	57.3	23.1	28.6	78.3
ULOPS (Ours)	61.5	68.3	58.1	35.3	45.3	79.8

Superscripts Th and St refer to *thing* and *stuff* classes, respectively. All metrics are reported in %.

ambiguous regions, leading to more reliable unknown object segmentation and improved performance. This uncertainty-aware learning strategy not only enhances UQ but also contributes to a boosted segmentation quality for known classes. The combination of instance-aware embedding and prototype association further strengthens our model’s ability to distinguish between known and unknown categories. The strong PQTh scores across different settings demonstrate our approach’s effectiveness to process thing classes while maintaining comparable performance on stuff classes (PQSt).

We observe a general decline in known PQ across all methods when shifting from Vocabulary 1 to Vocabulary 2. However, our approach maintains a strong advantage in unknown detection. Specifically, our method boosts UQ up to 50.1% on SemanticKITTI and 25.9% on KITTI-360, outperforming all tested baselines. Notably, 4D-PLS and PolarSeg-Panoptic also show improved UQ scores under Vocabulary 2, likely due to the reduced number of unknown categories simplifying the task.

In Tab. II, we further assess our method on nuScenes [21]. Our method leverages training unknown labels to guide uncertainty modeling, which outperforms methods based on K+1 supervision alone. Similarly, in Tab. III, we report performances on KITTI-360 using our defined Vocabulary Unseen. We observe a similar trend, with our model consistently outperforming all baselines for both known and unknown panoptic segmentation. These results underscore the advantages of integrating uncertainty modeling with structured feature learning. Our uncertainty-driven losses enable the network to effectively delineate the boundaries between known and unknown regions, leading to a more robust and balanced segmentation performance across both known and unknown objects.

D. Ablation Study

In this section, we present two ablation experiments on key components of our network. First, we investigate various uncertainty estimation techniques without supervision to demonstrate that uncertainty estimation is a promising research direction for LiDAR open-set panoptic segmentation. Next, we examine the impact of our proposed losses, which leverage available unknown labels to refine the network’s uncertainty estimation.

1) *Comparison of Uncertainty Estimation Methods:* In Tab. IV, we compare the performance of four uncertainty estimation methods, namely Softmax, DUQ [55], SNGP [56],

TABLE IV
KITTI-360 PERFORMANCE COMPARISON OF ANNOTATION-FREE
UNCERTAINTY ESTIMATION METHODS.

Method	Vocabulary Unseen		Vocabulary 1	
	PQ	UQ	PQ	UQ
Softmax	51.7	0.5	51.3	0.8
DUQ [55]	54.6	5.6	53.2	12.9
SNGP [56]	57.9	14.6	56.7	22.8
Dirichlet [45]	60.4	27.9	59.1	31.2

TABLE V
IMPACT OF UNCERTAINTY-DRIVEN LOSSES ON KITTI-360
PERFORMANCE.

Method	Vocabulary Unseen		Vocabulary 1	
	PQ	UQ	PQ	UQ
Proto-Unknowns [17]	58.4	15.1	57.1	23.2
ULOPS	60.4	27.9	59.1	31.2
+ Uniform Evidence	61.0	31.7	59.7	34.5
+ Adaptive Uncertainty	61.1	32.3	59.9	35.1
+ Contrastive Uncertainty	61.5	35.3	60.6	38.6

and our Dirichlet-based approach implemented in ULOPS. The results are displayed for Vocabulary Unseen and Vocabulary 1. We note that only the uncertainty estimation module is replaced for this experiment in our ULOPS architecture. The baseline approach Softmax yields moderate PQ scores (51.7% and 51.3%) but almost negligible UQ, clearly indicating its inability to distinguish unknown objects. DUQ improves UQ modestly (5.6% and 12.9%), while SNGP further boosts both PQ and UQ, suggesting that uncertainty-aware techniques enhance open set detection. Notably, the Evidential approach achieves the highest performance, with a PQ of 60.4% and UQ of 27.9% on Vocabulary 1, and a PQ of 59.1% and UQ of 31.2% on Vocabulary Unseen. Although both vocabularies are treated as unseen in this experiment (with Vocabulary Unseen being a subset of Vocabulary 1), the greater diversity among unknown objects in Vocabulary 1 forces the network to produce more pronounced uncertainty estimates, resulting in higher UQ scores, whereas the lower diversity in Vocabulary Unseen leads to milder uncertainty responses. Overall, these results confirm that uncertainty-aware learning significantly enhances open-set segmentation performance, with our Dirichlet-based approach proving especially effective when handling a broader range of unknown objects.

2) *Impact of Proposed Losses:* Tab. V presents the impact of our proposed uncertainty losses on the LiDAR open-set panoptic segmentation performance across two vocabulary settings. We first compare two baseline mechanisms for handling unknowns. The Proto-Unknowns baseline, following [17], is implemented in our ULOPS by removing the uncertainty estimation component and introducing a learnable global constant U , which serves as the score for not associating with any known prototype. In contrast, the ULOPS implicitly identifies unknowns through uncertainty estimation. Notably, the Association-Based Unknowns baseline yields a PQ of 58.4% and 57.1% with UQ at 15.1% and 23.2% on Vocabulary Unseen and Vocabulary 1 respectively. Meanwhile, the ULOPS model demonstrates an improved known-unknown

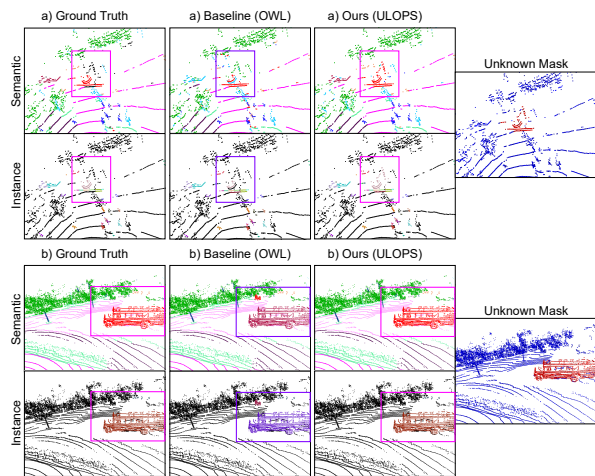


Fig. 3. Qualitative results of ULOPS compared to the OWL baseline for open-set LiDAR panoptic segmentation. Semantic and instance predictions within the pink box denote correct classifications, while those in the purple box indicate misclassifications.

separation (UQ of 27.9% and 31.2%), while also achieving improvement in PQ, indicating that leveraging uncertainty cues can generalize to unseen classes even without explicit unknown annotations. However, exposure to unknown samples significantly improves this separation. Incorporating Uniform Evidence Loss increases UQ (+3.8% on Vocabulary Unseen, +3.3% on Vocabulary 1), showing that enforcing a flat Dirichlet distribution for unknown voxels effectively raises per-voxel uncertainty. However, PQ remains relatively unchanged, suggesting that while the network becomes more uncertain about unknowns, it does not necessarily refine segmentation quality. Following, introducing Adaptive Uncertainty Separation Loss further enhances UQ (+0.6% and +0.6% over Uniform Evidence Loss), confirming that leveraging batch-level statistics ensures an improved distinction between known and unknown uncertainties. Notably, this improvement comes without a significant PQ drop, suggesting that the loss dynamically balances uncertainty separation between known and unknown uncertainties. Finally, Contrastive Uncertainty Loss achieves the most substantial gains, boosting UQ to 35.3% (+7.4%) and 38.6% (+7.4%) across the two vocabularies while also improving PQ. This validates our hypothesis that explicitly enforcing a margin-based separation between known and unknown uncertainties leads to a more structured and meaningful uncertainty landscape. The simultaneous PQ improvement suggests that this contrastive approach also enhances feature representations.

E. Qualitative Results

We qualitatively compare the performance of ULOPS with the best-performing baseline, OWL [18], as illustrated in Fig. 6. Both models successfully segment barriers in (a). However, OWL struggles to fully segment the construction vehicle, misclassifying parts of it as man-made structures or vegetation. In contrast, ULOPS correctly segments the vehicle, demonstrating improved separation between known and unknown objects. Similarly, in (b), OWL misclassifies

the unknown object as a truck and falsely detects parts of the vegetation as unknown. ULOPS produces a more accurate segmentation, avoiding these errors and providing better differentiation between open-set objects in the scene.

V. CONCLUSION

In this work, we introduced ULOPS, an uncertainty-guided open-set LiDAR panoptic segmentation framework. By leveraging Dirichlet-based evidential learning, our method explicitly models uncertainty to identify and separate unknown objects while maintaining segmentation accuracy for known categories. Our multi-task architecture integrates semantic segmentation with uncertainty estimation, instance embedding with prototype association, and instance center detection, enabling robust open-set perception. To enforce a structured distinction between known and unknown objects, we proposed three uncertainty-driven loss functions that improve the model's ability to detect and segment novel instances. Through extensive experiments on KITTI-360 and nuScenes datasets, we demonstrated that ULOPS consistently outperforms existing open-set LiDAR panoptic segmentation methods.

REFERENCES

- [1] R. Mohan, T. Elsken, A. Zela, J. H. Metzen, B. Staffler, T. Brox, A. Valada, and F. Hutter, "Neural architecture search for dense prediction tasks in computer vision," *International Journal of Computer Vision*, vol. 131, no. 7, pp. 1784–1807, 2023.
- [2] M. Luz, R. Mohan, A. R. Sekkat, O. Sawade, E. Matthes, T. Brox, and A. Valada, "Amodal optical flow," in *2024 IEEE International Conference on Robotics and Automation (ICRA)*. IEEE, 2024, pp. 14 677–14 684.
- [3] N. Vödisch, K. Petek, W. Burgard, and A. Valada, "Codeps: Online continual learning for depth estimation and panoptic segmentation," *Robotics: Science and Systems*, 2023.
- [4] D. Cattaneo and A. Valada, "Cmnext: Camera to lidar matching in the wild for localization and extrinsic calibration," *IEEE Transactions on Robotics*, 2025.
- [5] A. L. Ballardini, S. Fontana, D. Cattaneo, M. Matteucci, and D. G. Sorrenti, "Vehicle localization using 3d building models and point cloud matching," *Sensors*, vol. 21, no. 16, p. 5356, 2021.
- [6] K. Sirohi, R. Mohan, D. Büscher, W. Burgard, and A. Valada, "Efficientlps: Efficient lidar panoptic segmentation," *IEEE Trans. on Robotics*, vol. 38, no. 3, pp. 1894–1914, 2021.
- [7] J. Hindel, D. Cattaneo, and A. Valada, "Taxonomy-aware continual semantic segmentation in hyperbolic spaces for open-world perception," *IEEE Rob. and Auto. Let.*, vol. 10, no. 2, pp. 1904–1911, 2025.
- [8] R. Mohan, K. Kumaraswamy, J. V. Hurtado, K. Petek, and A. Valada, "Panoptic out-of-distribution segmentation," *IEEE Robotics and Automation Letters*, 2024.
- [9] M. Käppeler, K. Petek, N. Vödisch, W. Burgard, and A. Valada, "Few-shot panoptic segmentation with foundation models," in *Proc. IEEE Int. Conf. on Rob. and Auto.*, 2024, pp. 7718–7724.
- [10] N. Gosala, K. Petek, P. L. Drews-Jr, W. Burgard, and A. Valada, "Skyeye: Self-supervised bird's-eye-view semantic mapping using monocular frontal view images," in *Proc. IEEE Conf. Comput. Vis. Pattern Recog.*, 2023, pp. 14 901–14 910.
- [11] R. Mohan and A. Valada, "Perceiving the invisible: Proposal-free amodal panoptic segmentation," *IEEE Rob. and Auto. Let.*, vol. 7, no. 4, pp. 9302–9309, 2022.
- [12] B. Bešić, N. Gosala, D. Cattaneo, and A. Valada, "Unsupervised domain adaptation for lidar panoptic segmentation," *IEEE Rob. and Auto. Let.*, vol. 7, no. 2, pp. 3404–3411, 2022.
- [13] R. Mohan, D. Cattaneo, F. Drews, and A. Valada, "Progressive multi-modal fusion for robust 3d object detection," in *8th Annual Conference on Robot Learning*, 2024.
- [14] S. Vaze, K. Han, A. Vedaldi, and A. Zisserman, "Open-set recognition: A good closed-set classifier is all you need?" 2021.
- [15] Y. Guo, G. Camporese, W. Yang, A. Sperduti, and L. Ballan, "Conditional variational capsule network for open set recognition," in *Proc. of the IEEE/CVF Int. Conf. on Computer Vision*, 2021, pp. 103–111.
- [16] J. Sun and Q. Dong, "A survey on open-set image recognition," *arXiv preprint arXiv:2312.15571*, 2023.
- [17] K. Wong, S. Wang, M. Ren, M. Liang, and R. Urtasun, "Identifying unknown instances for autonomous driving," in *Conf. on Robot Learning*, 2020, pp. 384–393.
- [18] A. S. Chakravarthy, M. R. Ganesina, P. Hu, L. Leal-Taixé, S. Kong, D. Ramanan, and A. Osep, "Lidar panoptic segmentation in an open world," *Int. Journal of Computer Vision*, pp. 1–22, 2024.
- [19] S. Kong and D. Ramanan, "Opengan: Open-set recognition via open data generation," in *Proc. Int. Conf. Comput. Vis.*, 2021, pp. 813–822.
- [20] Y. Liao, J. Xie, and A. Geiger, "Kitti-360: A novel dataset and benchmarks for urban scene understanding in 2d and 3d," *IEEE Trans. on Pattern Analysis and Machine Intelligence*, vol. 45, no. 3, pp. 3292–3310, 2022.
- [21] W. K. Fong, R. Mohan, J. V. Hurtado, L. Zhou, H. Caesar, O. Beijbom, and A. Valada, "Panoptic nusenes: A large-scale benchmark for lidar panoptic segmentation and tracking," *IEEE Rob. and Auto. Let.*, vol. 7, no. 2, pp. 3795–3802, 2022.
- [22] Z. Xiao, W. Zhang, T. Wang, C. C. Loy, D. Lin, and J. Pang, "Position-guided point cloud panoptic segmentation transformer," *Int. Journal of Computer Vision*, vol. 133, no. 1, pp. 275–290, 2025.
- [23] X. Zhu, H. Zhou, T. Wang, F. Hong, Y. Ma, W. Li, H. Li, and D. Lin, "Cylindrical and asymmetrical 3d convolution networks for lidar segmentation," in *Proc. IEEE Conf. Comput. Vis. Pattern Recog.*, 2021, pp. 9939–9948.
- [24] Y. Zhang, Z. Zhou, P. David, X. Yue, Z. Xi, B. Gong, and H. Foroosh, "Polarnet: An improved grid representation for online lidar point clouds semantic segmentation," in *Proc. IEEE Conf. Comput. Vis. Pattern Recog.*, 2020, pp. 9601–9610.
- [25] K. Sirohi, S. Marvi, D. Büscher, and W. Burgard, "Uncertainty-aware lidar panoptic segmentation," in *2023 IEEE international conference on robotics and automation (ICRA)*. IEEE, 2023, pp. 8277–8283.
- [26] J. V. Hurtado, R. Mohan, W. Burgard, and A. Valada, "Mopt: Multi-object panoptic tracking," *arXiv preprint arXiv:2004.08189*, 2020.
- [27] Z. Zhou, Y. Zhang, and H. Foroosh, "Panoptic-polarnet: Proposal-free lidar point cloud panoptic segmentation," in *Proc. IEEE Conf. Comput. Vis. Pattern Recog.*, 2021, pp. 13 194–13 203.
- [28] M. Aygun, A. Osep, M. Weber, M. Maximov, C. Stachniss, J. Behley, and L. Leal-Taixé, "4d panoptic lidar segmentation," in *Proc. IEEE Conf. Comput. Vis. Pattern Recog.*, 2021, pp. 5527–5537.
- [29] E. Li, R. Razani, Y. Xu, and B. Liu, "Smac-seg: Lidar panoptic segmentation via sparse multi-directional attention clustering," in *Proc. IEEE Int. Conf. on Rob. and Auto.*, 2022, pp. 9207–9213.
- [30] S. Su, J. Xu, H. Wang, Z. Miao, X. Zhan, D. Hao, and X. Li, "Pups: Point cloud unified panoptic segmentation," in *Proc. of the AAAI Conf. on Artificial Intelligence*, vol. 37, no. 2, 2023, pp. 2339–2347.
- [31] B. Cheng, I. Misra, A. G. Schwing, A. Kirillov, and R. Girdhar, "Masked-attention mask transformer for universal image segmentation," in *Proc. IEEE Conf. Comput. Vis. Pattern Recog.*, 2022, pp. 1290–1299.
- [32] Y. Gu, Y. Huang, C. Xu, and H. Kong, "Maskrange: A mask-classification model for range-view based lidar segmentation," *arXiv preprint arXiv:2206.12073*, 2022.
- [33] A. Bendale and T. E. Boult, "Towards open set deep networks," in *Proc. IEEE Conf. Comput. Vis. Pattern Recog.*, 2016, pp. 1563–1572.
- [34] R. Mohan, J. Arce, S. Mokhtar, D. Cattaneo, and A. Valada, "Synmediverse: A multimodal synthetic dataset for intelligent scene understanding of healthcare facilities," *IEEE Robotics and Automation Letters*, 2024.
- [35] A. R. Sekkat, R. Mohan, O. Sawade, E. Matthes, and A. Valada, "Amodalsynthdrive: A synthetic amodal perception dataset for autonomous driving," *IEEE Robotics and Automation Letters*, 2024.
- [36] Z. Ge, S. Demyanov, Z. Chen, and R. Garnavi, "Generative openmax for multi-class open set classification," *arXiv preprint arXiv:1707.07418*, 2017.
- [37] L. Neal, M. Olson, X. Fern, W.-K. Wong, and F. Li, "Open set learning with counterfactual images," in *Proc. Springer Eur. Conf. Comput. Vis.*, 2018, pp. 613–628.
- [38] L. Ditria, B. J. Meyer, and T. Drummond, "Opengan: Open set generative adversarial networks," in *Proc. of the Asian Conf. on computer vision*, 2020.
- [39] X. Sun, Z. Yang, C. Zhang, K.-V. Ling, and G. Peng, "Conditional

- gaussian distribution learning for open set recognition,” in *Proc. IEEE Conf. Comput. Vis. Pattern Recog.*, 2020, pp. 13 480–13 489.
- [40] R. Yoshihashi, W. Shao, R. Kawakami, S. You, M. Iida, and T. Naemura, “Classification-reconstruction learning for open-set recognition,” in *Proc. IEEE Conf. Comput. Vis. Pattern Recog.*, 2019, pp. 4016–4025.
- [41] R. Krishnan, M. Subedar, and O. Tickoo, “Bar: Bayesian activity recognition using variational inference,” *arXiv preprint arXiv:1811.03305*, 2018.
- [42] W. Shi, X. Zhao, F. Chen, and Q. Yu, “Multifaceted uncertainty estimation for label-efficient deep learning,” *Adv. Neural Inform. Process. Syst.*, vol. 33, pp. 17 247–17 257, 2020.
- [43] A. Malinin and M. Gales, “Predictive uncertainty estimation via prior networks,” *Adv. Neural Inform. Process. Syst.*, vol. 31, 2018.
- [44] B. Charpentier, D. Zügner, and S. Günnemann, “Posterior network: Uncertainty estimation without ood samples via density-based pseudo-counts,” *Adv. Neural Inform. Process. Syst.*, vol. 33, pp. 1356–1367, 2020.
- [45] M. Sensoy, L. Kaplan, and M. Kandemir, “Evidential deep learning to quantify classification uncertainty,” *Adv. Neural Inform. Process. Syst.*, vol. 31, 2018.
- [46] D. Miller, L. Nicholson, F. Dayoub, and N. Sünderhauf, “Dropout sampling for robust object detection in open-set conditions,” in *Proc. IEEE Int. Conf. on Rob. and Auto.*, 2018, pp. 3243–3249.
- [47] J. Cen, P. Yun, S. Zhang, J. Cai, D. Luan, M. Tang, M. Liu, and M. Yu Wang, “Open-world semantic segmentation for lidar point clouds,” in *Proc. Springer Eur. Conf. Comput. Vis.*, 2022, pp. 318–334.
- [48] J. Hwang, S. W. Oh, J.-Y. Lee, and B. Han, “Exemplar-based open-set panoptic segmentation network,” in *Proc. IEEE Conf. Comput. Vis. Pattern Recog.*, 2021, pp. 1175–1184.
- [49] C. R. Qi, H. Su, K. Mo, and L. J. Guibas, “Pointnet: Deep learning on point sets for 3d classification and segmentation,” in *Proc. IEEE Conf. Comput. Vis. Pattern Recog.*, 2017, pp. 652–660.
- [50] O. Ronneberger, P. Fischer, and T. Brox, “U-net: Convolutional networks for biomedical image segmentation,” in *Proc. of the Int. Conf. on Medical image computing and computer-assisted intervention*, 2015, pp. 234–241.
- [51] B. De Brabandere, D. Neven, and L. Van Gool, “Semantic instance segmentation with a discriminative loss function,” *arXiv preprint arXiv:1708.02551*, 2017.
- [52] S. Learn, “Density-based spatial clustering of applications with noise.”
- [53] J. Winkens, R. Bunel, A. G. Roy, R. Stanforth, V. Natarajan, J. R. Ledsam, P. MacWilliams, P. Kohli, A. Karthikesalingam, S. Kohl *et al.*, “Contrastive training for improved out-of-distribution detection,” *arXiv preprint arXiv:2007.05566*, 2020.
- [54] J. Behley, M. Garbade, A. Milioto, J. Quenzel, S. Behnke, C. Stachniss, and J. Gall, “Semantickitti: A dataset for semantic scene understanding of lidar sequences,” in *Proc. Int. Conf. Comput. Vis.*, 2019, pp. 9297–9307.
- [55] J. Van Amersfoort, L. Smith, Y. W. Teh, and Y. Gal, “Uncertainty estimation using a single deep deterministic neural network,” in *Int. Conf. on machine learning*, 2020, pp. 9690–9700.
- [56] J. Liu, Z. Lin, S. Padhy, D. Tran, T. Bedrax Weiss, and B. Lakshminarayanan, “Simple and principled uncertainty estimation with deterministic deep learning via distance awareness,” *Adv. Neural Inform. Process. Syst.*, vol. 33, pp. 7498–7512, 2020.

Open-Set LiDAR Panoptic Segmentation Guided by Uncertainty-Aware Learning

- Supplementary Material -

Rohit Mohan¹, Julia Hindel¹, Daniele Cattaneo¹, Florian Drews², Claudius Gläser², Abhinav Valada¹

In this supplementary material, we provide additional details on the losses used to train the embedding decoder of ULOPS. We first describe the discriminative loss in Sec. S.1, followed by the prototype loss in Sec. S.2.

S.1. DISCRIMINATIVE LOSS

To enforce compact and separable instance embeddings, we adopt a discriminative loss composed of an intra-cluster pull term and an inter-cluster push term. These components jointly encourage embeddings belonging to the same instance to cluster tightly around a prototype, while ensuring that different instances remain well-separated in the embedding space.

The pull loss minimizes the distance between each voxel embedding and the prototype of its corresponding instance:

$$L_{\text{pull}} = \frac{1}{\sum_{c=1}^N |C_c|} \sum_{c=1}^N \sum_{v \in C_c} \|\phi_{\text{embed}}(v) - \mu_c\|^2, \quad (1)$$

where N is the number of instances, C_c denotes the set of voxels belonging to instance c , $\phi_{\text{embed}}(v) \in \mathbb{R}^d$ is the embedding vector of voxel v , and $\mu_c \in \mathbb{R}^d$ is the prototype (mean embedding) of instance c .

The push loss enforces separation between prototypes of different instances by penalizing those that are closer than a margin Δ :

$$L_{\text{push}} = \frac{1}{N(N-1)} \sum_{c \neq c'} \max\left(0, \Delta - \|\mu_c - \mu_{c'}\|^2\right), \quad (2)$$

where $\Delta > 0$ is a margin hyperparameter to prevent prototype collapse.

S.2. PROTOTYPE LOSS

To reinforce prototype consistency, we employ a prototype alignment loss, which encourages the learned prototype μ_c of each instance to match the average of the voxel embeddings assigned to that instance:

$$L_{\text{proto}} = \frac{1}{N} \sum_{c=1}^N \left\| \mu_c - \frac{1}{|C_c|} \sum_{v \in C_c} \Phi_{\text{embed}}(v) \right\|^2. \quad (3)$$

This loss stabilizes prototype updates and complements the pull and push terms by explicitly anchoring prototypes to their corresponding instance embeddings.

S.3. EMBEDDING LOSS

The total embedding loss is a weighted combination of the components introduced in Sec. S.1 and Sec. S.2:

$$L_{\text{embed}} = \lambda_{\text{pull}} L_{\text{pull}} + \lambda_{\text{push}} L_{\text{push}} + \lambda_{\text{proto}} L_{\text{proto}}, \quad (4)$$

where $\lambda_{\text{pull}}, \lambda_{\text{push}}, \lambda_{\text{proto}} \in \mathbb{R}_{\geq 0}$ are hyperparameters controlling the relative importance of each term. In our experiments, we set $\lambda_{\text{pull}} = 1$, $\lambda_{\text{push}} = 1$, and $\lambda_{\text{proto}} = 0.001$.

By jointly optimizing these objectives, the embedding decoder learns a representation space where embeddings of voxels belonging to the same instance form compact clusters around their prototype, while remaining well-separated from other instances.

¹ Department of Computer Science, University of Freiburg, Germany

² Bosch Research, Robert Bosch GmbH, Renningen, Germany